ORIGINAL ARTICLE

A Model of CatSper Channel Mediated Calcium Dynamics in Mammalian Spermatozoa

Sarah D. Olson[a,*], Susan S. Suarez[b], Lisa J. Fauci[a]

[a] *Mathematics Department, Tulane University, 6823 St. Charles Ave., New Orleans, LA 70118, USA*
[b] *Department of Biomedical Sciences, College of Veterinary Medicine, Cornell University, Ithaca, NY, USA*

Abstract CatSpers are calcium (Ca^{2+}) channels that are located along the principal piece of mammalian sperm flagella and are directly linked to sperm motility and hyperactivation. It has been observed that Ca^{2+} entry through CatSper channels triggers a tail to head Ca^{2+} propagation in mouse sperm, as well as a sustained increase of Ca^{2+} in the head. Here, we develop a mathematical model to investigate this propagation and sustained increase in the head. A 1-d reaction-diffusion model tracking intracellular Ca^{2+} with flux terms for the CatSper channels, a leak flux, and plasma membrane Ca^{2+} clearance mechanism is studied. Results of this simple model exhibit tail to head Ca^{2+} propagation, but no sustained increase in the head. Therefore, in this model, a simple plasma membrane pump-leak system with diffusion in the cytosol cannot account for these experimentally observed results. It has been proposed that Ca^{2+} influx from the CatSper channels induce additional Ca^{2+} release from an internal store. We test this hypothesis by examining the possible role of Ca^{2+} release from the redundant nuclear envelope (RNE), an inositol 1,4,5-trisphosphate (IP$_3$) gated Ca^{2+} store in the neck. The simple model is extended to include an equation for IP$_3$ synthesis, degradation, and diffusion, as well as flux terms for Ca^{2+} in the RNE. When IP$_3$ and the RNE are accounted for, the results of the model exhibit a tail to head Ca^{2+} propagation as well as a sustained increase of Ca^{2+} in the head.

Keywords Calcium · Reaction-diffusion · CatSper channels · Spermatozoa motility · Inositol 1,4,5-trisphosphate

Abbreviations

IP$_3$	inositol 1,4,5-trisphosphate
RNE	redundant nuclear envelope
IP$_3$R	inositol 1,4,5-trisphosphate receptor
Ca^{2+}	Calcium

*Corresponding author.
E-mail addresses: solson2@tulane.edu (Sarah D. Olson), sss7@cornell.edu (Susan S. Suarez), fauci@tulane.edu (Lisa J. Fauci).

[Ca^{2+}] Calcium concentration
cAMP cyclic adenosine monophosphate
PMCA plasma membrane Ca^{2+}-ATPase

1. Introduction

Intracellular calcium (Ca^{2+}) signaling has been studied and modeled for many years in somatic cells (Berridge, 2005). In spermatozoa, the exact mechanisms of Ca^{2+} signaling are unknown and are currently being investigated (Jimenez-Gonzalez et al., 2006). Experimentally, it has been shown that the intracellular Ca^{2+} concentration ([Ca^{2+}]) in sperm regulates motility and hyperactivation (Carlson et al., 2005; Ho and Suarez, 2001b; Suarez, 2008), capacitation (Visconti, 2009), and the acrosome reaction (Kirkman-Brown et al., 2003). Spermatozoa must undergo the acrosome reaction, the fusion of the acrosomal membrane with the outer plasma membrane (see Fig. 2), which requires increased intracellular [Ca^{2+}] in the head, to penetrate and fertilize the egg (Kirkman-Brown et al., 2003). Increases in intracellular [Ca^{2+}] can trigger sperm hyperactivation, motility characterized by an increased flagellar bend amplitude and beat asymmetry, enabling the sperm to reach the oocyte and to penetrate the oocyte zona pellucida (Quill et al., 2003; Ren et al., 2001; Stauss et al., 1995; Ho and Suarez, 2001b). Capacitation is a series of fast and slow processes that imparts on the sperm the ability to fertilize the egg (Visconti, 2009). Initiation and regulation of sperm motility have been observed as a result of changes in intracellular cyclic adenosine monophosphate (cAMP), Ca^{2+}, and pH (Aoki et al., 1999; Ishijima et al., 2006; Marquez and Suarez, 2004; Marquez et al., 2007). Note that these changes may be dependent on extracellular Ca^{2+} concentration.

Signals are produced by the opening of Ca^{2+} channels in the plasma membrane, in the membrane of Ca^{2+} storage organelles, or both, acting together (Berridge, 2005; Felix, 2005; Jimenez-Gonzalez et al., 2006). Channel activity can be modulated by other ions and enzymes, influencing the rates and direction of ion flow through channels and exchangers, which in turn affect intracellular pH, Ca^{2+}, and other second messengers (Darszon et al., 2001). Ion channels are key signaling elements in spermatozoa since motility, maturation, and the acrosome reaction can also be inhibited by certain channel blockers (Publicover and Barratt, 1999). Spermatozoa possess intricate mechanisms for regulation and coordination of Ca^{2+} signals (Jimenez-Gonzalez et al., 2006).

The exact mechanisms and pathways by which Ca^{2+} controls motility in a sperm flagellum are not completely known, but the importance of intracellular [Ca^{2+}] on motility and hyperactivation has been established (Felix, 2005; Ishijima et al., 2006; Smith, 2002; Suarez, 2008). Using a Ca^{2+} sensitive fluorescent dye, intracellular [Ca^{2+}] was observed to be higher in the head and in the flagellar midpiece of hyperactivated sperm, as compared to nonhyperactivated sperm (Suarez et al., 1993). Suarez et al. (1993, 2008) hypothesized that increases in intracellular [Ca^{2+}] initiates and maintains hyperactivation.

The CatSper family of proteins form heterotetrameric, pH, and voltage dependent Ca^{2+} permeable ion channels that are sperm specific and required for male fertility (Carlson et al., 2005; Quill et al., 2003; Qi et al., 2007; Ren et al., 2001; Xia et al., 2007). The CatSpers are located on the plasma membrane of the principal piece, the largest segment of the flagellum (Fig. 2) (Quill et al., 2003; Ren et al., 2001; Xia et al., 2007). Four different proteins have been identified: CatSper-1 (Ren et al.,
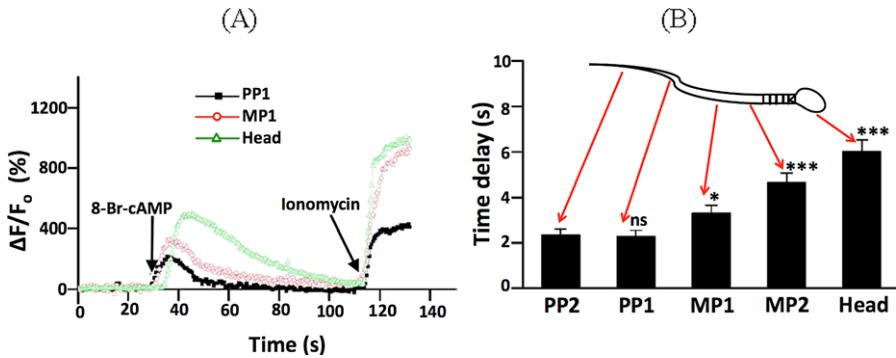
Fig. 1 Experimental results of Xia et al. (2007), (A) representative time courses of the relative $[Ca^{2+}]$ change at fixed locations in the principal piece (PP1), midpiece (MP1), and head from sperm with normal functioning CatSper channels, (B) averaged time difference between the application of 8-Br-cAMP and the onset of the fluorescence change in the indicated subregions. Notation for significance of the time delay: *ns* is not statistically significant ($P > 0.05$) compared with PP2, * is statistically significant ($P < 0.05$), and *** is statistically significant with $P < 0.001$. (Reproduced with permission from Xia et al., 2007.) (Color figure online.)

2001), -2 (Quill et al., 2003), -3 and -4 (Jin et al., 2007; Lobley et al., 2003). Elimination of any of the four CatSper proteins decreases sperm motility over time, therefore, CatSper channels may be involved in regulating basal motility (Qi et al., 2007; Quill et al., 2003). Through targeted disruption of each of the CatSper proteins, it has been shown that all four are necessary for hyperactivation (Carlson et al., 2005; Qi et al., 2007).

In several experiments, it has been observed that the application of extracellular cell permeant cyclic nucleotide analogs induces a rapid increase of intracellular $[Ca^{2+}]$ in the cytosol of the sperm (Kobori et al., 2000; Ren et al., 2001; Xia et al., 2007). The extracellular cyclic nucleotide analog diffuses into the cytosol of the sperm where it undergoes enzymatic conversion to a cyclic nucleotide. The direct mechanism by which the cyclic nucleotide activates Ca^{2+} influx is not known, but this response is not observed in CatSper-1 null sperm (Carlson et al., 2003). Previous patch clamp recordings suggest that cyclic nucleotides do not directly open CatSper channels (Kirichok et al., 2006; Ren et al., 2001). It has been proposed that Ca^{2+} entry through CatSper channels after the application of cell permeant cyclic nucleotides analogs could be due to channel facilitation instead of direct gating (Carlson et al., 2003).

In experiments performed by Xia et al. (2007), relative intracellular $[Ca^{2+}]$ along the length of mouse sperm was recorded using a Ca^{2+} sensitive fluorescent dye after the application of a cell permeable cAMP analog. As in Suarez et al. (1993), the relative intracellular $[Ca^{2+}]$ was observed to be higher in the head. The results from Xia et al. (2007) are shown in Fig. 1. The relative intracellular $[Ca^{2+}]$ is recorded as the relative increase in fluorescence intensity (ΔF) with respect to the basal value of fluorescence in the sperm (F_o), i.e., $\Delta F/F_o = 0$ corresponds to no change in relative $[Ca^{2+}]$ from the resting level. It is noted that $\Delta F/F_o$, the relative intracellular $[Ca^{2+}]$, may not correspond linearly to the actual $[Ca^{2+}]$ in the cytosol of the sperm, but it does give a qualitative understanding of how $[Ca^{2+}]$ is changing within different regions of the sperm.

In Fig. 1(A), the relative intracellular [Ca^{2+}] observed after the application of 8-Br-cAMP is shown at three locations along the flagellum. Increases in intracellular [Ca^{2+}] started in the principal piece and were then followed by increases in the midpiece and the head (Xia et al., 2007). The Ca^{2+} influx initiates a Ca^{2+} signal starting in the principal piece that propagates toward the head, as reflected by the time differences between the application of 8-Br-cAMP and the onset of increased fluorescence, shown in panel B. There was a time difference of 3.2 seconds between the increase in relative [Ca^{2+}] in the head and principal piece, along with a 1 second time difference within regions of the midpiece. A significant time difference for increase in [Ca^{2+}] was not seen in the principal piece. Similar results were obtained with the application of 8-Br-cGMP, another cyclic nucleotide analog, whose role in mammalian sperm has not been clearly established. In comparison, when ionomycin, a Ca^{2+} ionophore that facilitates the transport of Ca^{2+} across the plasma membrane, is applied to the extracellular medium, the fluorescence was immediate in all regions along the length of the sperm. Also, no significant Ca^{2+} increase was seen in sperm from CatSper null mutants. Xia et al. (2007) hypothesized that 8-Br-cAMP indirectly opens the CatSper channels, Ca^{2+} enters the principal piece through the CatSper channels, and the resulting Ca^{2+} influx triggers a tail to head propagation. The main question they proposed is: Can diffusion alone account for the sustained increase of Ca^{2+} in the head or is there some type of Ca^{2+} release that takes place due to the influx of Ca^{2+} from the CatSper channels?

The goal of this work is to introduce a mathematical model of Ca^{2+} dynamics in mammalian sperm that can be used to examine the effects of hypothesized mechanisms on the spatial and temporal evolution of Ca^{2+} along the flagellum. These mechanisms include diffusion and nonlinear fluxes that may depend on other signaling molecules. Here, we examine CatSper mediated Ca^{2+} dynamics and determine that additional Ca^{2+} release from an internal store is necessary to account for the sustained increase of Ca^{2+} in the head observed by Xia et al. (2007).

2. Ca^{2+} dynamics

2.1. Spatial model

Figure 2 shows a schematic of a sperm comprised of a head, neck, and tail regions. Given the spermatozoa geometry, we propose the following 1-dimensional reaction-diffusion model of Ca^{2+} dynamics ($t > 0, 0 < x < L$),

$$\frac{\partial C}{\partial t} = D_{Ca} \frac{\partial^2 C}{\partial x^2} + J_{CAT}(x,t) - J_{PMCA}(x,t) + J_{PP,leak}(x,t) \qquad (1)$$

where $C(x,t)$ (μM) is the Ca^{2+} concentration, D_{Ca} is the effective diffusion coefficient (μm^2 s^{-1}), and all of the time and space varying Ca^{2+} fluxes are denoted with a J (μM s^{-1}). Specifically, J_{CAT} is the flux through the CatSper channels into the sperm, J_{PMCA} is the flux out of the sperm through the plasma membrane channel, and $J_{PP,leak}$ is the leak of Ca^{2+} into the sperm from the surrounding medium. We will use a constant diffusion coefficient, assuming that the microtubules, fibers, mitochondria, acrosome, and nucleus do not create barriers to diffusion of Ca^{2+} in the cytoplasm (Fig. 2). In this model, we assume that the net Ca^{2+} flux across the mitochondria in the midpiece is negligible in comparison to the fluxes outlined in Eq. (1) (refer to the Discussion) (Ho and Suarez, 2003;
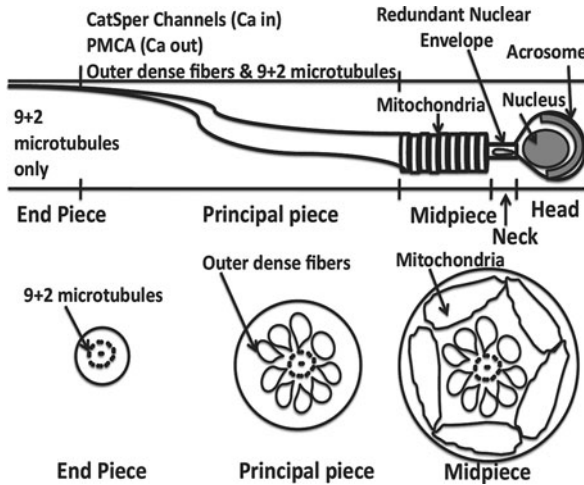
Fig. 2 Schematic of sperm geometry and regions.

Wennemuth et al., 2003). In this initial model, we wish to explore whether a simple pump-leak system with diffusion can account for the sustained Ca^{2+} increase in the head. Therefore, we do not account for any Ca^{2+} release from the acrosome and redundant nuclear envelope (RNE), Ca^{2+} stores in sperm (refer to Discussion) (Herrick et al., 2005; Ho and Suarez, 2003). Note that in this model Ca^{2+} buffering is included implicitly in the model by treating all fluxes as effective fluxes and using a small effective Ca^{2+} diffusion coefficient, similar to that of Sneyd et al. (2002, 2003). This is equivalent to assuming that all of the Ca^{2+} buffers that are present are immobile, unsaturated, and have fast Ca^{2+} binding kinetics (Wagner and Keizer, 1994). For the present time, we are neglecting the fact that the sperm are motile during the experiment.

2.2. Fluxes

The principal piece is the longest segment of the tail and contains the $9 + 2$ microtubules, the outer dense fibers, fibrous sheath, and Ca^{2+} channels relevant to Ca^{2+} clearance and motility (Pesch and Bergmann, 2006; Wennemuth et al., 2003; Xia et al., 2007). CatSper channels are located on the plasma membrane of the principal piece (Quill et al., 2003; Ren et al., 2001; Xia et al., 2007). In the experiment performed by Xia et al. (2007), a cell permeant cAMP analog, 8-Br-cAMP, was applied extracellularly, and Ca^{2+} entered through CatSper channels after the subsequent diffusion of the analog into the cytosol and enzymatic conversion into cAMP. The cAMP is proposed to facilitate the opening of the CatSpers channels (Carlson et al., 2003). The activation of CatSper channels may be enhanced by phosphorylation, similar to other voltage gated Ca^{2+} channels (Nolan et al., 2004; Sperelakis et al., 1994). Specifically, in myocardial cells and vascular smooth muscle cells, elevation of cAMP increases the probability of the Ca^{2+} channel being open and the mean open time of the channel. In these cells, the elevation of cAMP activates a cAMP dependent protein kinase (PKA), which may phosphorylate the channel protein itself or a regulatory protein, increasing the number of channels in the phosphorylated or

active form (Sperelakis et al., 1994). A sperm specific catalytic subunit of PKA, $C\alpha_2$, has been identified and is speculated to be required for CatSper dependent Ca^{2+} entry (Nolan et al., 2004). It is noted that PKA is localized to the flagellum through the anchoring of the $RII\alpha$ subunits, the predominant R subunit in mature sperm, by A-kinase anchoring proteins (Burton and McKnight, 2007; Nolan et al., 2004).

Since the exact mechanism of how cAMP facilitates the opening of CatSper channels is not known, we model the flux of Ca^{2+} through the CatSper channels in a phenomenological manner. We assume that the flux through the CatSper channel, J_{CAT} ($\mu M\,s^{-1}$),

$$J_{CAT}(x, t) = \begin{cases} 0 & x \notin PP \\ k_{CAT} \cdot \mathbb{O}(t) \cdot Ca_{EXT} & x \in PP \end{cases} \tag{2}$$

is proportional to the fraction of open CatSper channels, $\mathbb{O}(t)$, and the $[Ca^{2+}]$ in the surrounding medium, Ca_{EXT} (μM). It is assumed that Ca_{EXT} is constant, similar to Blum et al. (2000). The rate constant of the CatSper channel is k_{CAT} (s^{-1}) and PP denotes the principal piece. The fraction of open CatSper channels along the principal piece is described by the following differential equation,

$$\frac{\partial \mathbb{O}}{\partial t} = v_1 A(1 - \mathbb{O}) - v_2 \mathbb{O} \tag{3}$$

where $0 \leq \mathbb{O} \leq 1$. Here, $A(t)$ is the concentration of cAMP (μM) and v_1 and v_2 are rate constants. Once the cell permeant cAMP analog is introduced into the surrounding medium, it diffuses into the cytosol where it is enzymatically converted to cAMP. The cAMP then facilitates the opening of the CatSper channels. The channels are opening at a rate v_1 ($\mu M^{-1}\,s^{-1}$), proportional to the amount of cAMP present in the cytosol and the channels are closing at a rate v_2 (s^{-1}), proportional to the number of open channels. When the fraction of open channels reaches one, no more channels are being opened. The setup of Eq. (3) is similar to that of Washington et al. (2004), modeling the fraction of open voltage sensitive Ca^{2+} channels in the cell membrane. The time dependent concentration of cAMP, $A(t)$, is modeled as

$$\frac{\partial A}{\partial t} = -a_{deg} A \tag{4}$$

where we assume simple first order degradation kinetics of the cAMP, similar to Dougherty et al. (2005), governed by the degradation parameter a_{deg} (s^{-1}). The degradation of cAMP by cyclic nucleotide phosphodiesterases (PDEs), enzymes that hydrolyze cyclic nucleotides, play an important role in controlling resting state levels of cAMP (Lefievre et al., 2000; Tasken and Aandahl, 2004). We do not model the resting concentration of cAMP in the cytosol, assuming that it is at the same constant concentration before the application of the 8-Br-cAMP extracellularly and after all of the enzymatically converted 8-Br-cAMP is degraded. The dynamics of 8-Br-cAMP diffusion from the medium into the cytosol are not accounted for in this model. In fact, we assume that the 8-Br-cAMP instantaneously diffuses into the cytosol where it is enzymatically converted to cAMP.

A plasma membrane Ca^{2+}-ATPase pump (PMCA) has been localized from antibody staining studies along the principal piece of the flagellum in mouse sperm (Okunade et al., 2004). There are four PMCA isoforms, of which 90% are PMCA-4 in sperm (Okunade et al., 2004). It is noted that PMCA-4 null mouse sperm are unable to undergo hyperactivation and have severely impaired sperm motility (Okunade et al., 2004;

Schuh et al., 2004). The PMCA performs the major task of Ca^{2+} clearance, exporting excess cytoplasmic Ca^{2+} and importing one or two protons from the extracellular medium at the expense of ATP (Wennemuth et al., 2003). In sperm, when the PMCA is depressed due to changes in proton concentration or pH of medium in bath, other mechanisms can clear small amounts of cytoplasmic Ca^{2+}, but only to an intermediate level (Wennemuth et al., 2003). Therefore, we only model the PMCA, the primary mode of Ca^{2+} clearance in the principal piece. The PMCA is often modeled as a Hill function, where cooperative binding is represented with a Hill coefficient greater than one (Hong et al., 2008; Sneyd, 2002; Sneyd et al., 2003). We model the flux through the PMCA, J_{PMCA} ($\mu M\,s^{-1}$), as

$$J_{PMCA}(x,t) = \begin{cases} 0 & x \notin PP \\ V_{PMCA} \frac{C(x,t)^{n_{pm}}}{C(x,t)^{n_{pm}} + k_{PMCA}^{n_{pm}}} & x \in PP \end{cases} \tag{5}$$

where V_{PMCA} ($\mu M\,s^{-1}$) is the maximal velocity of Ca^{2+} extrusion by the pump, k_{PMCA} (μM) is the Ca^{2+} concentration for half activation of the pump, and n_{pm} is the Hill coefficient.

Experimentally, it was determined by Wennemuth et al. that there was a constant leak into the cytosol from the surrounding medium through the plasma membrane Wennemuth et al. (2003). Currently, there is little information about the magnitude of the leak in reference to location along the flagellum. Therefore, this was modeled as a constant leak only in the principal piece, $J_{PP,leak}$ ($\mu M\,s^{-1}$).

2.3. Numerical methods

We solved the model equations on a 1-d grid with uniform spatial size $\Delta x = 0.01$ μm. For all of the simulations, a fixed geometry is used for the sperm, with an overall length of $L = 120$ μm, with $x = 0$ and $x = L$ corresponding to the beginning of the head and the end of the tail, respectively. This length was chosen based on reference values for mouse sperm, and each of the regions were set as follows: head $= 10$ μm, neck $= 2$ μm, midpiece $= 20$ μm, principal piece $= 80$ μm, and end piece $= 8$ μm (Cummins and Woodall, 1985; Pesch and Bergmann, 2006). The principal piece (PP) corresponds to 32–112 μm and the neck corresponds to 10–12 μm. Initially, the Ca^{2+} concentration is set to a resting level along the entire length and no flux boundary conditions are prescribed at $x = 0$ and $x = 120$ μm. A second-order centered difference was used for $\partial^2 C/\partial x^2$ and a second-order discretization of $\partial C/\partial t$ was used. A semiimplicit method was employed, using an implicit time discretization for the diffusion terms and explicit discretization of the Ca^{2+} flux terms. The differential equation for open CatSper channels, Eq. (3), was solved explicitly. The equations were solved at each time step, $\Delta t = 0.01$ s.

2.4. Parameters for simulations

We assume that the sperm is at a resting/basal level of Ca^{2+} at the start of the experiment, zero CatSper channels are open prior to the application of the 8-Br-cAMP, and there is no 8-Br-cAMP in the medium prior to its application at $t = 5$ s. That is,

$$C(x,0) = Ca^*, \quad \mathbb{O}(0) = 0, \quad A(t) = \begin{cases} 0 & t < 5 \\ A^* & t = 5 \end{cases} \tag{6}$$

are the initial conditions prescribed. The parameters Ca_{EXT}, and A^* are estimated from the experiment by Xia et al. (2007). It is assumed that all of the 8-Br-cAMP diffuses instantaneously through the plasma membrane and is enzymatically converted to cAMP in the cytosol. Therefore, we set $A^* = 100$ μM at $t = 5$ s, estimated from Xia et al. (2007) where 10 μl of a 1 mM solution of 8-Br-cAMP is added into an imaging chamber with an approximate total volume of 100 μl. The rate, a_{deg}, corresponding to the degradation of cAMP was held constant at 0.1 s^{-1}, which was estimated from experimental data where degradation was measured in sperm (Lefievre et al., 2000). We use a degradation rate at the upper end since we are assuming no loss of 8-Br-cAMP in the medium surrounding the sperm and enzymatic conversion of all 8-Br-cAMP to cAMP in the cytosol. It is noted that the calculated initial resting values for intracellular [Ca^{2+}] were in the range of 0.1 to 0.25 μM and were as high as 2 μM after successive depolarizations in experiments by Wennemuth et al. (2000, 2003). In experiments with detergent demembranated bull sperm, the [Ca^{2+}] of the medium was approximately 0.2–1 μM in sperm exhibiting hyperactivated motility and motility was arrested at 1 mM (Ho et al., 2002).

No measurements of the PMCA and leak parameters ($J_{\mathrm{PP,leak}}$, V_{PMCA}, k_{PMCA}, n_{pm}) in the principal piece are available for sperm. We choose to fix $n_{pm} = 2$ based on previous experimental and modeling studies on other cell types (Camello et al., 1996; Sneyd et al., 2003). The balance between the leak and PMCA fluxes sets the steady state, therefore, the three remaining parameters were chosen to obtain agreement with the experimentally observed steady state [Ca^{2+}] in the entire length of the sperm before the application of 8-Br-cAMP. Simulations were run to determine the PMCA and leak parameters using literature values obtained for other cell types as a starting point. The parameters for this model are outlined in Table 1. Note that all parameters were chosen to agree with resting [Ca^{2+}] and to ensure [Ca^{2+}] stayed within experimentally observed levels (Ho et al., 2002; Wennemuth et al., 2000, 2003).

For each of the graphs showing Ca^{2+} concentrations and time delays, corresponding to data from Fig. 1, the locations were set as: H = 5 μm, MP2 = 20 μm, MP1 = 28 μm, PP1 = 36 μm, and PP2 = 45 μm based off of the locations presented in Xia et al. (2007). In the results from Xia et al. (2007), the time delays were calculated as the time differences between the application of the 8-Br-cAMP and the onset of fluorescence change, which was defined as the time point when $\Delta F/F_o$ started to have a steep rise. For all results shown in the following sections, this corresponds to a rise of 0.01 μM in 1 s. This rate of change is reasonable given experimental results by Wennemuth et al. (2000) where they reported 0.04 μM s^{-1} as an average rate of intracellular Ca^{2+} rise when depolarizing Ca^{2+} channels in sperm.

3. Results

Representative results of the model are shown in Fig. 3. The parameters used for the CatSper channels are outlined in Table 1. As can be seen in Fig. 3(A) for $D_{\mathrm{Ca}} = 20$, when the 8-Br-cAMP is placed into the medium surrounding the sperm at $t = 5$ s, Ca^{2+} rises first in the principal piece, where the CatSper channels are located. After $t = 5$ s, the Ca^{2+} influx in the principal piece propagates along the length of the sperm. In Fig. 3(B)–(C) the time course of cAMP concentration and its effect on the number of open CatSpers can

Table 1 Parameters values for the initial model presented in Sect. 2

Parameter		Value	References
CatSper parameters			
k_{CAT}	Basal rate of CatSper	3.5×10^{-4} s^{-1}	–
v_1	Rate of CatSpers opening	0.005 s^{-1}	–
v_2	Rate of CatSpers closing	0.07 s^{-1}	–
PMCA parameters			
V_{PMCA}	Maximal velocity of PMCA	0.75 µM s^{-1}	(a)
n_{pm}	Hill coefficient of PMCA	2	(a), (b), 1.9 in (c)
k_{PMCA}	[Ca^{2+}] for 1/2 activation of PMCA	0.2 µM	(a), (c)
Ca^{2+} parameters			
$J_{PP,leak}$	Ca^{2+} leak into cytosol via PP	0.15 µM s^{-1}	–
D_{Ca}	Ca^{2+} diffusion coefficient	20 µm^2 s^{-1}	(d), (e)
Ca_{EXT}	[Ca^{2+}] in medium	2000 µM	(f)
Ca^*	Resting [Ca^{2+}]	0.1 µM	0.1–0.25 in (g)
cAMP parameters			
a_{deg}	Rate of cAMP degradation	0.1 s^{-1}	(h)
A^*	[cAMP] in cytosol at $t = 5$ s	100 µM	(f)

Note. References: (a) Hong et al. (2008), (b) Sneyd et al. (2003), (c) Camello et al. (1996), (d) Allbritton et al. (1992), (e) Sneyd et al. (1995), (f) estimated from experiment of Xia et al. (2007), (g) Wennemuth et al. (2003), (h) estimated from Lefievre et al. (2000). For those parameters where a reference was not listed, the parameter was chosen so as to agree with the trends of the data of Xia et al. (2007) and experimentally observed resting levels of Ca^{2+}

be seen. (Note that the x-axis for both graphs (B) and (C) start at $t = 5$ s.) When the 8-Br-cAMP is enzymatically converted to cAMP in the cytosol, it facilitates the opening of CatSper channels and is quickly degraded. The fraction of open channels reaches a peak around 0.73 at about $t = 11$ s and then channels close as cAMP is degraded. The time difference between application of the cAMP and resulting increase of Ca^{2+} influx above 0.01 µM s^{-1} is shown in panel (D) for three Ca^{2+} diffusion coefficients. For $D_{Ca} = 20$, the time difference is much greater in the head than in the principal piece, similar to the results seen by Xia et al. (2007). A 0.7 s, 2.3 s, and 8.7 s time difference is observed between the principal piece and MP1, MP2, and H, respectively. Three important qualitative aspects to note are: (1) the Ca^{2+} concentration reaches a maximum in the principal piece and is always less than this value in the head, (2) a sustained increase in Ca^{2+} is not observed in the head, and (3) the time difference for increased Ca^{2+} from principal piece to head is longer than that observed by Xia et al. (2007). Using a range of values for the parameters v_1, v_2, and k_{CAT}, similar behavior was noted (results not shown).

Could increasing the effective diffusion coefficient of Ca^{2+} result in a sustained, higher [Ca^{2+}] in the head? In this model, Ca^{2+} is only being removed from the sperm to the surrounding media by the PMCA in the principal piece, therefore, if the Ca^{2+} is able to diffuse into the head fast enough, it could potentially reach a higher concentration there since there is no removal of Ca^{2+} accounted for in this region. In Fig. 4(A)–(B), the effective Ca^{2+} diffusion coefficient is increased, which would correspond to a decrease in
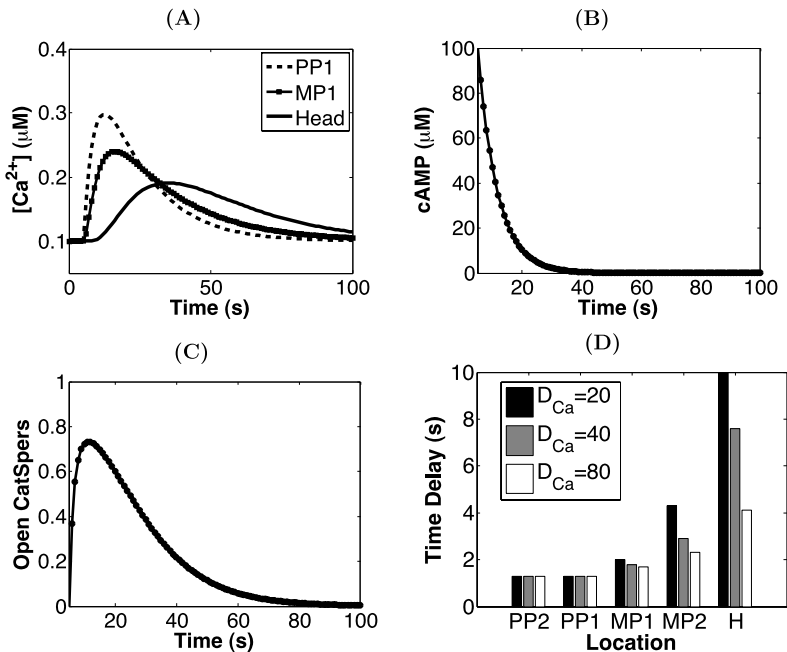
(A)

(B)

(C)

(D)

Fig. 3 Numerical simulations of: (A) $[Ca^{2+}]$ at PP1, MP1, and the head for 100 s where 8-Br-cAMP is applied at $t = 5$ s, (B) [cAMP], (C) fraction of open CatSper channels, (D) time delay from application of 8-Br-cAMP at 5 s and the increased change in $[Ca^{2+}]$ in each of the five regions.
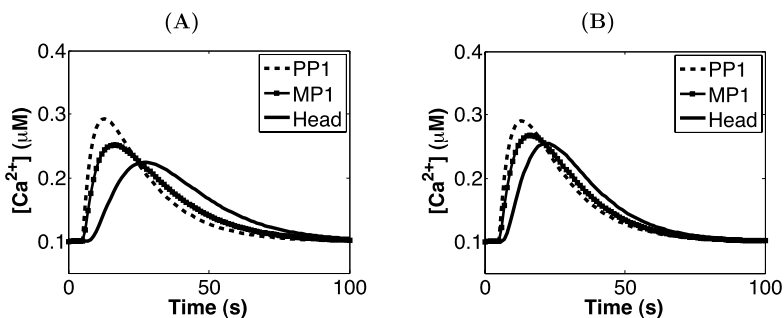
(A)

(B)

Fig. 4 Numerical simulations of $[Ca^{2+}]$ at PP1, MP1, and the head for 100 s where 8-Br-cAMP is applied at $t = 5$ s using the following effective Ca^{2+} diffusion coefficients: (A) $D_{Ca} = 40$, (B) $D_{Ca} = 80$.

Ca^{2+} binding to buffers or other proteins in the cytosol. The $[Ca^{2+}]$ still achieves its maximum in the principal piece. As the diffusion coefficient is increased, the maximal $[Ca^{2+}]$ in the head increases but is not sustained. The diffusion coefficient was also increased up to 300 $\mu m^2 s^{-1}$, corresponding to free Ca^{2+} with no buffering (Wagner and Keizer, 1994). Similarly, there is not a sustained increase in Ca^{2+} in the head (results for these simulations not shown). The corresponding time differences for Ca^{2+} propagation from the

principal piece to the head are shown in Fig. 3(D). As the effective diffusion coefficient is increased, the time difference between increased Ca^{2+} concentrations in the principal piece and head decreases.

4. Extended model of Ca^{2+} dynamics

In the first model, it was found that a higher sustained $[Ca^{2+}]$ in the head was not observed. Here, we explore the role of Ca^{2+} entering through the CatSper channels as a signal to trigger Ca^{2+} release from an intracellular store, which was proposed by Xia et al. (2007) as a possible explanation for the increase in Ca^{2+} in the head.

The redundant nuclear envelope (RNE) is a Ca^{2+} store at the base of the flagellum located in the neck and is found in a variety of mammalian sperm (Ho and Suarez, 2001a, 2003). Immunolabeling verified that type I inositol 1,4,5-trisphosphate (IP_3) receptors and calreticulin, a high capacity Ca^{2+} binding protein associated with IP_3 receptor (IP_3R) containing Ca^{2+} stores in somatic cells, are located in the neck region containing the RNE (Ho and Suarez, 2003). In other experiments, thapsigargin, a Ca^{2+}-ATPase inhibitor that depletes intracellular Ca^{2+} stores, induced an increase in intracellular $[Ca^{2+}]$ great enough to switch on hyperactivation in the absence of available external Ca^{2+} (Ho and Suarez, 2003). Therefore, increases in intracellular $[Ca^{2+}]$ during hyperactivation have been hypothesized to be partially from the release of Ca^{2+} in the RNE through an IP_3 gated channel (Ho and Suarez, 2001a, 2003). In this extended model, we wish to explore the possible role of IP_3 and the IP_3 gated Ca^{2+} store, the RNE, in the neck region.

4.1. Extended spatial model

The 1-dimensional spatial model for the Ca^{2+}, $C(x, t)$ (μM), and IP_3, $P(x, t)$ (μM) concentrations is as follows ($t > 0$, $0 < x < L$),

$$\frac{\partial C}{\partial t} = D_{Ca}\frac{\partial^2 C}{\partial x^2} + J_{CAT} - J_{PMCA} + J_{PP,leak} + J_{RNE,out} - J_{RNE,in} \tag{7}$$

$$\frac{\partial P}{\partial t} = D_P\frac{\partial^2 P}{\partial x^2} + IP_{3_{prod}} - IP_{3_{deg}} \tag{8}$$

where all of the Ca^{2+} fluxes are denoted with a J (μM s^{-1}). The extended model now includes Ca^{2+} flux terms out of the RNE, $J_{RNE,out}$, and into the RNE, $J_{RNE,in}$. We examined a simplified model that assumed a constant background of IP_3 to calculate the additional Ca^{2+} fluxes from the RNE. While this simple model did exhibit a sustained increase in Ca^{2+} in the head, the Ca^{2+} concentration was sustained for a much longer time scale than that seen in experiments for parameter choices within the range of literature values. Therefore, in the extended model, we account for the concentration of IP_3 with a reaction-diffusion equation (8), where D_P is the effective diffusion coefficient of IP_3 (μm s^{-2}). The production and degradation of IP_3 are accounted for in the terms $IP_{3_{prod}}$ and $IP_{3_{deg}}$, respectively. As in the first model, Ca^{2+} buffering is included implicitly and diffusion is assumed to be constant along the length of the sperm. In this extended model, we are only accounting for Ca^{2+} release from the RNE. It is assumed that the acrosome reaction and

CatSper mediated Ca^{2+} dynamics are two different processes, with unique mechanisms for initiation; therefore, we neglect any Ca^{2+} release from the acrosomal store in the current model.

4.2. Additional fluxes, degradation, and synthesis

As a result of the influx of Ca^{2+} through CatSper channels, we hypothesize that the synthesis of IP_3 is also increased. In experiments, sperm treated with a Ca^{2+} ionophore A23187 led to the activation of phospholipase C (PLC), generating diacylglycerol (DAG) and IP_3 in a variety of mammalian sperm (Felix, 2005; Roldan, 1998). It was also observed that DAG formation did not occur with the presence of Ca^{2+} channel blockers, giving evidence that activation of PLC and the subsequent synthesis of IP_3 and DAG takes place after Ca^{2+} entry in sperm (Roldan, 1998). In other cell types, production of IP_3 is due to the activation of PLC (Rhee, 2001), which can be governed by a receptor mediated process or directly from the Ca^{2+} ions, with varying sensitivities (Rebecchi and Pentyala, 2000; Smrcka et al., 1991; Taylor and Exton, 1987). Studies have also shown that cAMP can mediate or trigger stimulation of PLC to generate IP_3 (Schmidt et al., 2001). Several isoforms of PLC have been identified in mammalian sperm, including PLCδ4 (Fukami et al., 2003), PLCζ (Swann et al., 2004), and PLCβ in the head and midpiece (Kuroda et al., 1999; Walensky and Snyder, 1995).

Since the exact mechanism and PLC isoform involved in upregulation of IP_3 synthesis is not known, we assume that IP_3 is being synthesized in the neck, the location of the RNE. The following equation is used to model the synthesis of IP_3, $IP_{3_{prod}}$ ($\mu M\,s^{-1}$),

$$IP_{3_{prod}}(x,t) = \begin{cases} 0 & x \notin \text{Neck} \\ v_s \cdot A(t) \cdot \frac{C(x,t)}{C(x,t)+k_{PLC}} & x \in \text{Neck} \end{cases} \tag{9}$$

where $A(t)$ (μM) is the concentration of cAMP, k_{PLC} (μM) characterizes the sensitivity of PLC to $[Ca^{2+}]$ and v_S (s^{-1}) is the maximal rate of IP_3 production. It is assumed that the stimulation of PLC to generate IP_3 is triggered or mediated by cAMP and is also sensitive to Ca^{2+} concentration. This equation allows the IP_3 concentration to initially increase after the application of 8-Br-cAMP with increasing levels of Ca^{2+}. As time increases, the IP_3 production will decrease due to a decreased concentration of cAMP. When there is no cAMP present, it is assumed that activation of PLC is not being triggered by cAMP, therefore, no IP_3 is generated. It is assumed that prior to the opening of the CatSper channels the synthesis of IP_3 in the neck is zero. Previous studies have modeled IP_3 production in a similar fashion (Hong et al., 2008; Meyer and Stryer, 1988b, 1991). IP_3 is degraded by enzymes such as IP_3 3-kinase and 5-phosphatase in the cytosol (Pattni and Banting, 2004; Sims and Allbritton, 1998). We assume that the degradation of IP_3, $IP_{3_{deg}}$ ($\mu M\,s^{-1}$), occurs in the neck and obeys the following equation:

$$IP_{3_{deg}}(x,t) = p_{deg}P(x,t) \tag{10}$$

where p_{deg} (s^{-1}) is the degradation constant, similar to the models of Blum et al. (2000) and Hong et al. (2008).

We assume that the IP_3 receptors located on the RNE behave in a similar fashion to that of the endoplasmic reticulum (ER), which has been modeled in many frameworks. Previous experimental studies of IP_3 receptors and Ca^{2+} channels in the ER have examined the

domains of the IP$_3$ receptor (Meyer et al., 1990), the conductance levels at which it opens (Watras et al., 1991), and effective binding affinity of IP$_3$ with increased Ca^{2+} (Joseph et al., 1989). From these studies, many models of IP$_3$ gated Ca^{2+} release have been developed that assume Ca^{2+} directly affects the binding of IP$_3$. Systems of equations for the probability of an IP$_3$ gated channel in the ER being open have been developed (Sneyd et al., 2003), but due to a lack of experimental data at this point for this particular channel in the RNE of mammalian spermatozoa, we choose to take a simpler approach following Atri et al. (1993).

As in previous models for Xenopus and endothelial cells (Atri et al., 1993; Sneyd et al., 1995), the probability of the IP$_3$ receptor being open, Pr_{IP_3R}, is modeled in a phenomonological manner. We assume that the IP$_3$ receptor has three binding domains, one for IP$_3$ and two for Ca^{2+}. The probability of the IP$_3$ receptor being open, Pr_{IP_3R}, is dependent on the local Ca^{2+} concentration, $C(x,t)$ (μM), and the local IP$_3$ concentration, $P(x,t)$ (μM) (Sneyd et al., 1995):

$$Pr_{IP_3R}(x,t) = p_1 p_2 p_3 = \left(\frac{(P(x,t))^{n_p}}{(P(x,t))^{n_p} + (k_1)^{n_p}} \right) \left(b + \frac{(1-b)C(x,t)}{k_2 + C(x,t)} \right) h \qquad (11)$$

where n_p is the Hill coefficient and p_3 is governed by a slow variable h:

$$\tau_h \frac{\partial h}{\partial t} = \frac{k_3^2}{k_3^2 + C(x,t)^2} - h \qquad (12)$$

In Eq. (11), the proportion of receptors activated by IP$_3$ in the first domain is p_1, p_2 is the proportion of receptors having Ca^{2+} bound in the second domain, and $1-p_3$ is the proportion of receptors with Ca^{2+} bound in domain 3, i.e., p_3 is the proportion of receptors that have not been inactivated by Ca^{2+} in domain 3. The equations for p_1 and p_2 describe the binding of IP$_3$ in domain 1 and the binding and activation of the receptor by Ca^{2+} in domain 2, respectively. The binding and inactivation of domain 3 by Ca^{2+} is described by the term h, governed by Eq. (12). As Ca^{2+} increases, h gets smaller, decreasing to steady state with time constant τ_h (s^{-1}). The parameters in Eqs. (11)–(12) are described in Table 2.

We model the flux of Ca^{2+} out of the RNE, $J_{RNE,out}$ (μM s^{-1}) using the following equation:

$$J_{RNE,out}(x,t) = \begin{cases} 0 & x \notin \text{Neck} \\ V_{RNE}Pr_{IP_3R}(x,t) + V_{RNE,leak} & x \in \text{Neck} \end{cases} \qquad (13)$$

where V_{RNE} is the Ca^{2+} flux when all IP$_3$ receptors are open and activated on the RNE membrane (μM s^{-1}) and $V_{RNE,leak}$ is the Ca^{2+} leak across the RNE membrane (μM s^{-1}). It is assumed that the Ca^{2+} concentration in the RNE is large enough to sustain this flux out of the RNE. For this model, $V_{RNE,leak}$ is assumed to be constant. This type of equation has been used to model flux of Ca^{2+} out of the ER in previous models (Sneyd et al., 1995).

A secretory pathway Ca^{2+}-ATPase (SPCA) has been localized to the rear head of sperm and is likely to play a role in clearance of Ca^{2+} released from the RNE store (Bedu-Addo et al., 2008; Harper et al., 2005). We account for the uptake of Ca^{2+} into the RNE,

Table 2 Additional parameters for extended model presented in Sect. 4

Parameter		Value	References
IP$_3$ parameters			
D_P	IP$_3$ diffusion coefficient	300 μm^2 s^{-1}	(a)
v_s	Rate of IP$_3$ production	0.015 μM s^{-1}	–
$p_{\deg}$	Degradation rate of IP$_3$	2.5 s^{-1}	2.5 in (b), 2 in (c)
P^*	Resting [IP$_3$]	0 μM	–
Ca^{2+} parameters			
k_{PLC}	Sensitivity of PLC to Ca^{2+}	0.7 μM	(b)
V_{RNE}	Maximal Ca^{2+} flux	8.5 μM s^{-1}	3 in (d), 8.1 in (e)
$V_{RNE,leak}$	Ca^{2+} leak across RNE	0.145 μM s^{-1}	0.15 in (d)
IP$_3$R parameters			
n_p	Hill coefficient IP$_3$ binding	3	(d)
k_1	K_m for IP$_3$ binding to its R	0.05 μM	0.01 in (d), (f)
			0.026 and 1.6 in (g)
b	Fraction of act IP$_3$R	0.11	(d), (e), (h)
k_2	K_m for act of IP$_3$R by Ca^{2+}	0.7 μM	0.7 in (e), (h)
τ_h	Time for IP$_3$R inact by Ca^{2+}	0.2 s	(d), (i)
k_3	K_m for inact of R by Ca^{2+}	0.7 μM	(d), (e), (h)
SPCA parameters			
V_{SPCA}	Maximal velocity of SPCA	0.3 μM s^{-1}	0.286 in (j)
n_{sp}	Hill coefficient for SPCA	1	(e), (j), (k)
k_{SPCA}	[Ca^{2+}] for 1/2-act. of SPCA	0.1 μM	(e), (j)

Note: K_m = concentration at half maximal rate, act = activated, inact = inactivated, R = receptors, stim = stimulation. References: (a) Allbritton et al. (1992), (b) Hong et al. (2008), (c) Keizer and De Young (1992), (d) Sneyd et al. (1995), (e) Atri et al. (1993), (f) Meyer et al. (1988a), (g) Walensky and Snyder (1995), (h) Parys et al. (1992), (i) Finch et al. (1991), (j) Roose et al. (2006), (k) Dode et al. (2005)

$J_{RNE,in}$ (μM s^{-1}), via the following equation:

$$J_{RNE,in}(x,t) = \begin{cases} 0 & x \notin \text{Neck} \\ V_{SPCA} \cdot \frac{C(x,t)^{n_{sp}}}{k_{SPCA}^{n_{sp}} + C(x,t)^{n_{sp}}} & x \in \text{Neck} \end{cases} \tag{14}$$

where V_{SPCA} (μM s^{-1}) is the maximal velocity of the pump, k_{SPCA} (μM) is the concentration of Ca^{2+} where half-maximal uptake into the RNE occurs, and n_{sp} is the Hill coefficient. This form of equation for the flux of Ca^{2+} into the ER has been used in previous models to account for sarcoplasmic-endoplasmic reticulum Ca-ATPase (SERCA) pumps (Atri et al., 1993; Roose et al., 2006; Sneyd et al., 1995). We assume that this equation will account for the SPCA pump and any other fluxes of Ca^{2+} into the RNE.

4.3. Numerical methods and parameters

The extended model, Eqs. (7)–(8), were solved on the same grid in a similar fashion as described for Eq. (1), with no flux boundary conditions at $x = 0$ and $x = 120$ μm for

both C and P. The differential equation for h, Eq. (12), was solved explicitly. The initial conditions prescribed are the same as in Eq. (6) with the addition of the following:

$$P(x, 0) = P^*, \qquad h(0) = 1 \tag{15}$$

i.e., we assume that the sperm is at a resting/basal level of IP$_3$, P^*, and that none of the IP$_3$ receptors have been deactivated by Ca^{2+}. The principal piece (PP) corresponds to 32–112 μm and the neck corresponds to 10–12 μm.

Since the basal or resting level of IP$_3$ was not known for sperm, it was assumed to be zero. It is assumed that the IP$_3$ is synthesized in the neck and binds to the IP$_3$ receptors on the RNE, triggering Ca^{2+} to be released. From previous experimental studies, it has been shown that bovine sperm IP$_3$ receptors have properties similar to that of IP$_3$ receptors on the bovine adrenal cortex and adrenal medullar chromaffin cells (Minelli et al., 2000). It has also been observed that the IP$_3$ receptors in sperm have a high density, with IP$_3$ binding affinities that range from 0.026–0.75 μM in different mammalian species of sperm (Kuroda et al., 1999; Minelli et al., 2000; Walensky and Snyder, 1995). Staining studies have identified type I (Minelli et al., 2000; Ho and Suarez, 2001a; Walensky and Snyder, 1995) and type III (Kuroda et al., 1999) IP$_3$ receptors in mammalian sperm. The SPCA pump has been observed to transport Ca^{2+} with an affinity similar to that of ER SERCA pumps (Wuytack et al., 2002). The parameters governing Eq. (11) are outlined in Table 2 and were determined based on the above factors along with literature values from other cell types.

Before simulations of the extended model were completed, the constant leak flux out of the RNE, $V_{\text{RNE,leak}}$, and the RNE SPCA parameters in Eq. (14) had to be determined. The Hill coefficient was fixed, $n_{sp} = 1$, based on previous experimental and modeling studies (Dode et al., 2005). The other parameters ($V_{\text{RNE,leak}}$, V_{SPCA}, and k_{SPCA}) were varied within the range of literature values and chosen so as to obtain agreement with experimentally observed steady states. The values of these fixed parameters along with all other parameters from the extended model are shown in Table 2.

5. Results for extended model

Representative results for the model are shown in Fig. 5(A)–(B) for $D_{\text{Ca}} = 20$. In Fig. 5(A), it can be seen that the head reaches a maximum [Ca^{2+}] that is greater than the principal piece and is sustained at a higher concentration than the principal piece. At $t = 5$ s when the 8-Br-cAMP is applied, the facilitated opening of CatSper channels occurs in the principal piece, letting Ca^{2+} into the sperm. Note that since the CatSper dynamics are independent of the RNE and the same parameters were used, the time course for the fraction of open CatSper channels and concentration of cAMP remains the same as in the first model, shown in Fig. 3(B)–(C). As this is happening, the cAMP and Ca^{2+} are mediating the synthesis of IP$_3$.

The increase in [IP$_3$] then triggers Ca^{2+} release from the RNE, which is governed by the probability of the channel being open, Pr_{IP_3R}, a product of three proportions, p_1, p_2, and p_3 described in Eq. (11). In Fig. 5(B), each of these quantities is plotted at a fixed location in the neck for $t = 5$–100 s. The concentration of IP$_3$ governs p_1, which starts off at zero and increases as IP$_3$ is synthesized and then decreases down to zero as the
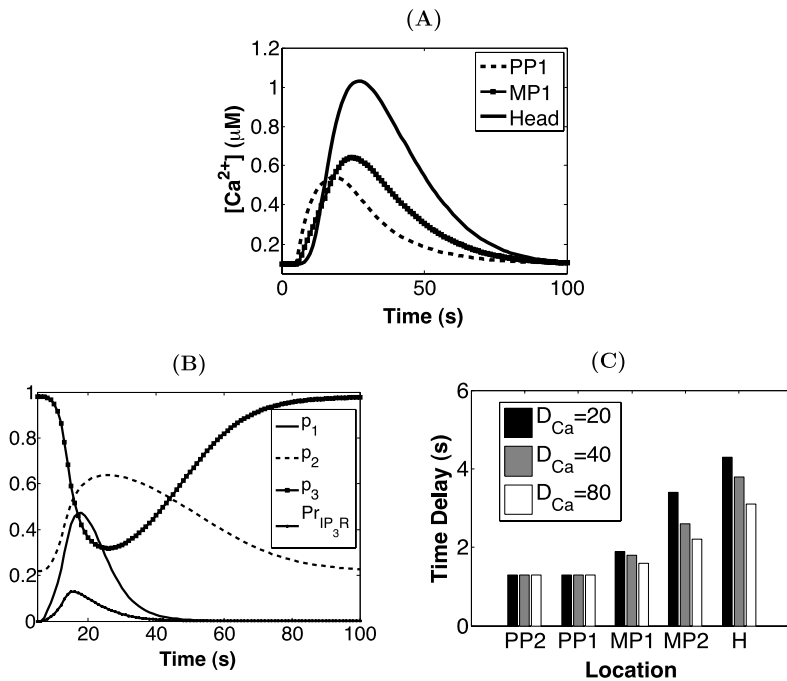
Fig. 5 Numerical simulations of the extended model accounting for IP$_3$ and induced Ca^{2+} release from the RNE: (A) [Ca^{2+}] at PP1, MP1, and the head for 100 s where cAMP is applied at $t = 5$ s, (B) p$_1$, p$_2$, p$_3$, and Pr$_{IP_3R}$ at a fixed location in the neck ($x = 11$ μm) for $t = 5$–100 s, (C) time differences from application of 8-Br-cAMP at 5 s to change in [Ca^{2+}] in each of the five regions.

[IP$_3$] decreases back to zero due to decreased synthesis of IP$_3$ and degradation of IP$_3$. The second proportion, p_2 is governed by the [Ca^{2+}], increasing as more Ca^{2+} propagates to the neck region and as Ca^{2+} is being released from the RNE. The inactivation of the IP$_3$ receptor occurs as the [Ca^{2+}] increases and is lowest around $t = 25$ s. These three proportions govern the probability of the IP$_3$ receptor being open, which is also shown in this plot. The IP$_3$ receptor starts off closed, then increases to a maximum around $t = 15$ s, and decreases back to zero.

The time differences for Ca^{2+} to propagate and increase in concentration along the flagellum is in agreement with the experimental data of Xia et al. (2007). In Fig. 5(C), for $D_{Ca} = 20$, approximately 1.3 s after the time of application of the 8-Br-cAMP, the [Ca^{2+}] rises similarly throughout the principal piece. There is a time difference in Ca^{2+} propagation from the principal piece to parts of the midpiece with MP1 and MP2 having time delays of 0.6 and 2.1 s from the application of 8-Br-cAMP, respectively. The head has the longest time difference to Ca^{2+} increase, which is 3 s. This is more than half of the time delay that was shown in Fig. 3(B). This is due to the increase in synthesis of IP$_3$ in the neck, which then causes Ca^{2+} release from the IP$_3$ gated Ca^{2+} channels on the RNE. In Fig. 5(C), as the diffusion coefficient of Ca^{2+} is increased, a similar tail to head propagation of Ca^{2+} is exhibited with decreasing time differences for increased Ca^{2+} in the head. The time differences for Ca^{2+} propagation and the sustained increase of Ca^{2+}

in the head were exhibited for a variety of parameters as long as there was sufficient IP_3 to bind to the first domain of the RNE.

In this extended model, we remark that simulations were first run with a nonzero resting level of IP_3 and zero synthesis and degradation of IP_3. The leak fluxes in the RNE required to achieve a resting level of Ca^{2+} before the application of 8-Br-cAMP, were also calculated. Using these leak fluxes, a sustained increase of Ca^{2+} in the head was observed for some parameters, but the Ca^{2+} did not decrease back to a resting level on the right time scale. Therefore, in this model, it is necessary to have IP_3 synthesized after the application of the 8-Br-cAMP and subsequent degradation back to a resting level of IP_3. Since the leak parameters are determined to achieve a steady state and the basal level of IP_3 was unknown in sperm, the basal level (initial condition) of IP_3 was chosen to be zero in the simulations presented in Fig. 5.

6. Discussion

Through the use of these simple one-dimensional models, we are able to numerically simulate Ca^{2+} entry through CatSper channels due to the application of 8-Br-cAMP, following the experimental setup of Xia et al. (2007). In both models, we observed a tail to head Ca^{2+} propagation. The first model was unable to capture the higher and sustained $[Ca^{2+}]$ in the head that were observed in experiments. The extended model was used to explore the role of Ca^{2+} entering through the CatSper channels as a signal to trigger Ca^{2+} release from an intracellular store. Numerical simulations of an IP_3 gated Ca^{2+} store in the neck region, the RNE, qualitatively agree with the experimental data by Xia et al. (2007). The head had a sustained increase in $[Ca^{2+}]$ and exhibited a tail to head propagation of Ca^{2+} with similar trends in time differences for increases in Ca^{2+} along the flagellum. In both models, the time delays for Ca^{2+} propagation varied from the experimental data of Xia et al. (2007). This could be partially due to the model assumption of constant diffusion. Nonconstant diffusion is likely based on the varying cellular structure throughout each of the regions. In addition, the sperm are moderately motile during the experiment of Xia et al. (2007), which could have an effect on diffusion and local $[Ca^{2+}]$.

Throughout the development of the initial and extended model, it must be noted that several assumptions were made. In both models, it was assumed that mitochondria, located in the midpiece, were not playing an active role in regulating intracellular $[Ca^{2+}]$, relative to other mechanisms. The mitochondria, which act as Ca^{2+} buffers, could potentially remove Ca^{2+} from the cytosol (Nicholls and Chalmers, 2005). In other cell types, the mitochondria Ca^{2+} uniporter (MCU) brings Ca^{2+} into the energized mitochondria only when Ca^{2+} is elevated above 0.5 μM (Gunter et al., 2000). In experiments completed by Wennemuth et al. (2003), prevention of Ca^{2+} uptake by the mitochondria in sperm had negligible effects on Ca^{2+} clearance in comparison to the PMCA. It is noted that in some cells, there is Ca^{2+} efflux from mitochondria that could supply Ca^{2+} to the surrounding cytosol (Nicholls and Chalmers, 2005). In experiments by Ho et al. (2003), blocking Ca^{2+} efflux from mitochondria with CGP-37157, an inhibitor of the Na^+/Ca^{2+} exchanger, did not alter $[Ca^{2+}]$ in the axoneme when hyperactivation was triggered using thapsigarin. These results led to the conclusion that Ca^{2+} was released from the RNE and diffused directly to the axoneme to trigger hyperactivation without active participation of the mitochondria (Ho and Suarez, 2003). In the current model we assume that the net Ca^{2+} flux

across the mitochondria in the midpiece was negligible in comparison to other channels and mechanisms, but further experimental studies are needed to determine under which physiological conditions these assumptions are valid.

We also assume that the Ca^{2+} release was IP_3 triggered and from the RNE in the neck region. The presence of IP_3R in mammalian sperm has been confirmed in many studies (Costello et al., 2009). It is noted that Ca^{2+} sensitivity by the IP_3 receptor itself could also be a reason for the Ca^{2+} induced Ca^{2+} release in the RNE (Taylor et al., 2009). The possible role of ryanodine receptors is less clear since studies have observed the presence of these receptors in human sperm (Harper et al., 2004; Lefievre et al., 2007) and no staining for ryanodine receptors using BODIPY FL-X ryanodine in bovine sperm has been reported (Ho and Suarez, 2001a). Since ryanodine receptors are sensitive to Ca^{2+}, it is possible that they play a role in amplifying or modulating Ca^{2+} signaling initiated by CatSper induced Ca^{2+} influx in some species of mammalian sperm. The acrosome, an IP_3 gated Ca^{2+} store in the head (Herrick et al., 2005), is not accounted for in this model. In experiments using Ca^{2+} store releasing agents to induce hyperactivation, it was found that the acrosome reaction was not induced by these treatments, therefore, the acrosomal store was assumed to not be involved (Ho and Suarez, 2001a). If a large enough Ca^{2+} flux out of the acrosome occurs, this will induce the acrosome reaction. It has also been observed by several researchers that CatSper null sperm from mice could undergo the acrosome reaction, but they could not hyperactivate (Quill et al., 2003; Ren et al., 2001; Xia et al., 2007). The $[Ca^{2+}]$ in the head and midpiece have also been observed to be greater in sperm that had undergone acrosome reaction (Suarez and Dai, 1995). Therefore, we are assuming that the acrosome reaction and CatSper mediated Ca^{2+} dynamics are two different processes, with unique mechanisms for initiation, and neglect any Ca^{2+} release from the acrosome in the current model.

CatSper channels have been implicated in regulating basal motility (Qi et al., 2007; Quill et al., 2003). In experiments by Marquez et al. (2007) with CatSper null sperm, the flagellar bend amplitudes were low, but could be raised to normal pre-hyperactivated levels with the application of thimerosal, which triggers release of Ca^{2+} from stores. Their experimental results indicated that resting levels of Ca^{2+} in CatSper null sperm are abnormally low and that the CatSper channels may play a role in regulating resting levels of Ca^{2+} and basal motility (Marquez et al., 2007). Since the sperm are moderately motile at the beginning of the Xia et al. (2007) experiment, there may be some CatSper channels open. We assume that the CatSper channels already open prior to the application of 8-Br-cAMP remain open for the time course of the experiment, and are therefore accounted for in the leak flux. It is also noted here that CatSper channels may be implicated in processes other than hyperactivation and basal motility. During mammalian fertilization, an increase in intracellular $[Ca^{2+}]$ is triggered by contact between the sperm and egg. In experiments, it was observed that Ca^{2+} entry through CatSper channels is required for zona pellucida (ZP) glycoprotein induced increases in intracellular $[Ca^{2+}]$ and is hypothesized to play a role in the acrosome reaction (Xia and Ren, 2009). For modeling purposes, we are assuming that this is a different signaling pathway initialized by ZP glycoproteins.

The motility of mammalian spermatozoa is an emergent property of a complex, dynamical system that couples chemical signaling, dynein force-generation dynamics, passive elastic properties of the sperm structure, and external fluid dynamics (e.g., Cosson, 1996; Ishijima et al., 2006; Smith, 2002; Suarez, 2008). Laboratory experiments and computational models together can provide insight into this complex system. The simple models of Ca^{2+} dynamics presented here should be viewed as a starting point that can elucidate

the relative importance of hypothesized Ca^{2+} transport mechanisms. It is our hope to couple these Ca^{2+} reaction-diffusion models with integrative mechanical models of sperm motility within a viscous, incompressible fluid (Dillon et al., 2007).

References

Allbritton, N.L., Meyer, T., Stryer, L., 1992. Range of messenger action of calcium ion and inositol 1,4,5-trisphosphate. Science 258, 1812–1815.

Aoki, F., Sakai, S., Kohmoto, K., 1999. Regulation of flagellar bending by cAMP and Ca^{2+} in hamster sperm. Mol. Reprod. Dev. 53, 777–83.

Atri, A., Amundson, J., Clapham, D., Sneyd, J., 1993. A single-pool model for intracellular calcium oscillations and waves in the Xenopus laevis oocyte. Biophys. J. 65, 1727–1739.

Bedu-Addo, K., Costello, S., Harper, C., Machado-Oliveira, G., Lefievre, L., Ford, C., Barratt, C., Publicover, S., 2008. Mobilisation of stored calcium in the neck region of human sperm—a mechanism for regulation of flagellar activity. Int. J. Dev. Biol. 52, 615–626.

Berridge, M.J., 2005. Unlocking the secrets of cell signalling. Annu. Rev. Physiol. 67, 1–21.

Blum, J.J., Reed, M.C., Janovick, J., Conn, P.M., 2000. A mathematical model quantifying GnRH-induced LH secretion from gonadotropes. Am. J. Physiol. Endocrinol. Metabol. 278, 263–272.

Burton, K.A., McKnight, S., 2007. PKA germ cells, and fertility. Physiol. 22, 40–46.

Camello, P.J., Gardner, O., Petersen, O.H., Tepikin, A.V., 1996. Calcium dependence of calcium extrusion and calcium uptake in mouse pancreatic acinar cells. J. Physiol. (Lond.) 490, 585–593.

Carlson, A.E., Westenbroek, R.E., Quill, T., Ren, D., Claphan, D.E., Hille, B., Garbers, D.L., Babcock, D.F., 2003. CatSper1 required for evoked Ca^{2+} entry and control of flagellar function in sperm. Proc. Natl. Acad. Sci. USA 100(25), 14864–14868.

Carlson, A.E., Quill, T.A., Westenbroek, R.E., Schuch, S.M., Hille, B., Babcock, D.F., 2005. Identical phenotypes of CatSper1 and CatSper2 null sperm. Int. J. Biol. Chem. 280, 32238–32244.

Cosson, J., 1996. A moving image of flagella: news and views on the mechanisms involved in axonemal beating. Cell Biol. Int. 20, 83–94.

Costello, S., Michelangeli, F., Nash, K., Lefievre, L., Morris, J., Machado-Oliveira, G., Barratt, C., Kirkman-Brown, J., Publicover, S., 2009. Ca^{2+}-stores in sperm: their identities and functions. Reproduction 138, 425–437.

Cummins, J.M., Woodall, P.F., 1985. On mammalian sperm dimensions. J. Reprod. Fertil. 75, 153–175.

Darszon, A., Beltran, C., Felix, R., Nishigaki, T., Trevino, C.L., 2001. Ion transport in sperm signaling. Dev. Biol. 240, 1–14.

Dillon, R., Fauci, L., Omoto, C., Yang, X., 2007. Fluid dynamic models of flagellar and ciliary beating. Ann. New York Acad. Sci. 1101(1), 494–505.

Dode, L., Andersen, J.P., Raeymaekers, L., Missiaen, L., Vilsen, B., Wuytack, F., 2005. Functional comparison between secretory pathway Ca^{2+}/Mn^{2+}-ATPase (SPCA) 1 and sarcoplasmic reticulum Ca^{2+}-ATPase (SERCA) 1 isoforms by steady-state and transient kinetic analyses. J. Biol. Chem. 280(47), 39124–39134.

Dougherty, D.P., Wright, G.A., Yew, A.C., 2005. Computational model of the cAMP-mediated sensory response and calcium-dependent adaptation in vertebrate olfactory receptor neurons. Proc. Natl. Acad. Sci. USA 102, 10415–10420.

Felix, R., 2005. Molecular physiology and pathology of Ca^{2+}-conducting channels in the plasma membrane of mammalian sperm. Reproduction 129, 251–262.

Finch, E.A., Turner, T.J., Goldin, S.M., 1991. Calcium as a coagonist of inositol 1,4,5-trisphosphate-induced calcium release. Science 252, 443–446.

Fukami, K., Yoshida, M., Inoue, T., Kurokawa, M., Fissore, R.A., Yoshida, N., Mikoshiba, K., Takenawa, T., 2003. Phospholipase Cδ4 is required for Ca^{2+} mobilization essential for acrosome reaction in sperm. J. Cell Biol. 161, 79–88.

Gunter, T.E., Buntinas, L., Sparagna, G., Eliseev, R., Gunter, K., 2000. Mitochondrial calcium transport: mechanisms and functions. Cell Calcium 28, 285–296.

Harper, C.V., Barratt, C.L., Publicover, S.J., 2004. Stimulation of human spermatozoa with progesterone gradients to stimulate approach to the oocyte. Induction of $[Ca_i^{2+}]$ oscillations and cyclical transitions in flagellar beating. J. Biol. Chem. 279, 46315–46325.

Harper, C., Wootton, L., Michelangeli, F., Lefievre, L., Barratt, C., Publicover, S., 2005. Secretory pathway Ca^{2+}-ATPase (SPCA1) Ca^{2+} pumps, not SERCAs, regulate complex [Ca^{2+}]$_i$ signals in human spermatozoa. J. Cell Sci. 118(8), 1673–1685.

Herrick, S.B., Schweissinger, D.L., Soo-Woo, K., Bryan, K.R., Mann, S., Cardullo, R.A., 2005. The acrosomal vesicle of mouse sperm is a calcium store. J. Cell Physiol. 202, C663–C671.

Ho, H.C., Suarez, S.S., 2001a. An inositol 1,4,5-trisphosphate receptor-gated intracellular Ca^{2+} store is involved in regulating sperm hyperactivated motility. Biol. Reprod. 65, 1606–1615.

Ho, H.C., Suarez, S.S., 2001b. Hyperactivation of mammalian spermatozoa: function and regulation. Reproduction 122, 519–526.

Ho, H.C., Suarez, S.S., 2003. Characterization of the intracellular calcium store at the base of the sperm flagellum that regulates hyperactivated motility. Biol. Reprod. 68, 1590–1596.

Ho, H.C., Granish, K.A., Suarez, S.S., 2002. Hyperactivated motility of bull sperm is triggered at the axoneme by Ca^{2+} and not cAMP. Dev. Biol. 250, 208–217.

Hong, D., Jaron, D., Buerk, D.G., Barbee, K.A., 2008. Transport-dependent calcium signaling in spatially segregated cellular caveolar domains. Am. J. Physiol., Cell Physiol. 294, C856–C866.

Ishijima, S., Mohri, H., Overstreet, J.W., Yudin, A.I., 2006. Hyperactivation of monkey spermatozoa is triggered by Ca^{2+} and completed by cAMP. Mol. Reprod. Dev. 73, 1129–1139.

Jimenez-Gonzalez, C., Michelangeli, F., Harper, C.V., Barratt, C.L.R., Publicover, S.J., 2006. Calcium signalling in human spermatozoa: a specialized 'toolkit' of channels, transporters, and stores. Hum. Reprod. Update 12, 253–267.

Jin, J., Jin, N., Zheng, H., Ro, S., Tafolla, D., Sanders, K.M., Yan, W., 2007. CatSper3 and CatSper4 are essential for sperm hyperactivated motility and male fertility in the mouse. Biol. Reprod. 77, 37–44.

Joseph, S.K., Rice, H.L., Williamson, J.R., 1989. The effect of external calcium and pH on inositol trisphosphate-mediated calcium release from cerebellum microsomal fractions. Biochem. J. 258, 261–265.

Keizer, J., De Young, G.W., Two roles for Ca^{2+} in agonist stimulated Ca^{2+} oscillations. Biophys. J. 61, 649–660.

Kirichok, Y., Navarro, B., Clapham, D.E., 2006. Whole cell patch clamp measurements of spermatozoa reveal an alkaline-activated Ca^{2+} channel. Nature 439, 737–740.

Kirkman-Brown, J.C., Barratt, C.L., Publicover, S.J., 2003. Zona pellucida and progesterone-induced Ca^{2+} signaling and acrosome reaction in human spermatozoa. J. Androl. 23, 306–315.

Kobori, H., Miyazaki, S., Kuwabara, T., 2000. Characterization of intracellular Ca^{2+} increase in response to progesterone and cyclic nucleotides in mouse spermatozoa. Biol. Reprod. 63, 113–120.

Kuroda, Y., Kaneko, S., Yoshimura, Y., Noazawa, S., Mikoshiba, K., 1999. Are there inositol 1,4,5-trisphosphate (IP$_3$) receptors in human sperm? Life Sci. 65(2), 135–143.

Lefievre, L., De Lamirande, E., Gagnon, C., 2000. The cyclic GMP-specific phosphodiesterase inhibitor, sildenafil, stimulates human sperm motility and capacitation but not acrosome reaction. J. Androl. 21, 929–937.

Lefievre, L., Chen, Y., Conner, S.J., Scott, J.L., Publicover, S.J., Ford, W.C., Barratt, C.L., 2007. Human spermatozoa contain multiple targets for protein S-nitrosylation: an alternative mechanism of the modulation of sperm function by nitric oxide? Proteomics 7, 3066–3084.

Lobley, A., Pierron, V., Reynolds, L., Allen, L., Michalovich, D., 2003. Identification of human and mouse CatSper3 and CatSper4 genes: characterisation of a common interaction domain and evidence for expression in testis. Reprod. Biol. Endocrinol. 1, 53–67.

Marquez, B., Suarez, S.S., 2004. Different signaling pathways in bovine sperm regulate capacitation and hyperactivation. Biol. Reprod. 70, 1626–1633.

Marquez, B., Ignotz, G., Suarez, S.S., 2007. Contributions of extracellular and intracellular Ca^{2+} to regulation of sperm motility: release of intracellular stores can hyperactivate CatSper1 and CatSper2 null sperm. Dev. Biol. 303, 214–221.

Meyer, T., Stryer, L., 1988b. Molecular model for receptor-stimulated calcium spiking. Proc. Natl. Acad. Sci. USA 85, 5051–5055.

Meyer, T., Stryer, L., 1991. Calcium spiking. Annu. Rev. Biophys. Biophys. Chem. 20, 153–174.

Meyer, T., Holowka, S., Stryer, L., 1988a. Highly cooperative opening of calcium channels by inositol 1,4,5-trisphosphate. Science 240, 653–656.

Meyer, T., Wensel, T., Stryer, L., 1990. Kinetics of calcium channel opening by inositol 1,4,5-trisphosphate. Biochemistry 29, 32–37.

Minelli, A., Allegrucci, C., Rosati, R., Mezzasoma, I., 2000. Molecular and binding characteristics of IP$_3$ receptors in bovine spermatozoa. Mol. Reprod. Dev. 56, 527–533.

Nicholls, D.G., Chalmers, S., 2005. The integration of mitochondrial calcium transport and storage. J. Bioenerg. Biomembranes 36(4), 1573–6881.

Nolan, M.A., Babcock, D.F., Wennemuth, G., Brown, W., Burton, K.A., McKnight, G.S., 2004. Sperm-specific protein kinase A catalytic subunit $C\alpha_2$ orchestrates cAMP signaling for male fertility. Proc. Natl. Acad. Sci. USA 101(37), 13483–13488.

Okunade, G.W., Miller, M.L., Pyne, G.J., Sutliff, R.L., O'Connor, K.T., Neumann, J.C., Andringa, A., Miller, D.A., Prasad, V., 2004. Targeted ablation of plasma membrane Ca^{2+}-ATPase (PMCA) 1 and 4 indicates a major housekeeping function for PMCA1 and a critical role in hyperactivated sperm motility and male fertility for PMCA4. J. Biol. Chem. 279(32), 33742–33750.

Parys, J.B., Sernett, S.E., DeLisle, S., Snyder, P.M., Welsh, M.J., Campbell, K.P., 1992. Isolation, characterization, and localization of the inositol 1,4,5-trisphosphate receptor protein in Xenopus laevis oocytes. Int. J. Biol. Chem. 267, 18776–18782.

Pattni, K., Banting, G., 2004. Ins(14,5)P_3 metabolism and the family of IP$_3$-3 kinases. Cell. Signal. 16(6), 643–654.

Pesch, S., Bergmann, M., 2006. Structure of mammalian spermatozoa in respect to viability, fertility, and cryopreservation. Micron 37, 597–612.

Publicover, S.J., Barratt, C.L., 1999. Voltage-operated Ca^{2+} channels and the acrosome reaction: which channels are present and what do they do? Hum. Reprod. 14, 873–879.

Qi, H., Moran, M.M., Navarro, B., Chong, J.A., Krapivinsky, G., Krapivinsky, L., Kirichok, Y., Ramsey, I.S., Quill, T.A., Clapham, D.E., 2007. All four CatSper ion channel proteins are required for male fertility and sperm cell hyperactivated motility. Proc. Natl. Acad. Sci. USA 104, 1219–1223.

Quill, T., Sugden, S.A., Rossi, K.L., Doolittle, L.K., Hammer, R.E., Garbers, D.L., 2003. Hyperactivated sperm motility driven by CatSper2 is required for fertilization. Proc. Natl. Acad. Sci. USA 100, 14869–14874.

Rebecchi, M.J., Pentyala, S.N., 2000. Structure function, and control of phosphoinositide-specific phospholipase. C. Physiol. Rev. 80, 1291–1335.

Ren, D., Navarro, B., Perez, G., Jackson, A.C., Hsu, S., Shi, Q., Tilly, J.L., Clapham, D.E., 2001. A sperm ion channel required for sperm motility and male fertility. Nature 413, 603–609.

Rhee, S.G., 2001. Regulation of phosphoinositide-specific phospholipase. C. Annu. Rev. Biochem. 70, 281–312.

Roldan, E.R.S., 1998. Role of phospholipases during sperm acrosomal exocytosis. Front. Biosci. 3, 1109–1119.

Roose, T., Chapman, S.J., Maini, P.K., 2006. A mathematical model for simultaneous spatio-temporal dynamics of calcium and inositol 1,4,5-trisphosphate in madin-darby canine kidney epithelial cells. Bull. Math. Biol. 68, 2027–2051.

Schmidt, M., Evellin, S., Paschal, A.O.W., von Dorp, F., Rehmann, H., Lomasney, J.W., Jakobs, K.H., 2001. A new phospholipase-C–calcium signalling pathway mediated by cyclic AMP and a Rap GTPase. Nat. Cell Biol. 3, 1020–1024.

Schuh, K., Cartwright, E.J., Jankevics, E., Bundschu, K., Liebermann, J., Williams, J.C., Armesilla, A.L., Emerson, M., Oceandy, D., Knobeloch, K.P., Neyses, L., 2004. Plasma membrane Ca^{2+} ATPase 4 is required for sperm motility and male fertility. J. Biol. Chem. 279, 28220–28226.

Sims, C.E., Allbritton, N.L., 1998. Metabolism of inositol 1,4,5-trisphosphate and inositol 1,3,4,5-tetrakisphosphate by the oocytes of Xenopus laevis. J. Biol. Chem. 273(7), 4052–4058.

Smith, E.F., 2002. Regulation of flagellar dynein by calcium and a role for an axonemal calmodulin and calmodulin dependent kinase. Mol. Biol. Cell 13, 3303–3313.

Smrcka, A.V., Helper, J.R., Brown, K.O., Sternweis, P.C., 1991. Regulation of polyphosphoinositide-specific phospholipase C activity by purified G_q. Science 251, 804–807.

Sneyd, J., 2002. Calcium excitability. In: Sneyd, J. (Ed.), An introduction to mathematical modeling in physiology, cell biology, and immunology. Proc. Sympos. Appl. Math. 59, 83–118.

Sneyd, J., Wetton, B.T.R., Charles, A.C., Sanderson, M.J., 1995. Intercellular calcium waves mediated by diffusion of inositol trisphosphate—a two-dimensional model. Am. J. Physiol. Cell Physiol. 268, C1537–C1545.

Sneyd, J., Tsaneva-Atanasova, K., Bruce, J.I.E., Straub, S.V., Giovannucci, D.R., Yule, D.I., 2003. A model of calcium waves in pancreatic and parotid acinar cells. Biophys. J. 85, 1392–1405.

Sperelakis, N., Xiong, X., Haddad, G., Masuda, H., 1994. Regulation of slow calcium channels of myocardial cells and vascular smooth muscle cells by cyclic nucleotides and phosphorylation. Mol. Cell. Biochem. 14, 103–117.

Stauss, C.R., Votta, T.J., Suarez, S.S., 1995. Sperm motility hyperactivation facilitates penetration of the hamster zona pellucida. Biol. Reprod. 53, 1280–1285.

Suarez, S.S., 2008. Control of hyperactivation in sperm. Hum. Reprod. Update 14, 647–657.

Suarez, S.S., Dai, X., 1995. Intracellular calcium reaches different levels in hyperactivated and acrosome-reacted hamster sperm. Mol. Reprod. Dev. 42(3), 325–333.

Suarez, S.S., Varosi, S.M., Dai, X., 1993. Intracellular calcium increases with hyperactivation in intact, moving hamster sperm and oscillates with the flagellar beat cycle. Proc. Natl. Acad. Sci. USA 90, 4660–4664.

Swann, K., Larman, M.G., Saunders, C.M., Lai, F.A., 2004. The cytosolic sperm factor that triggers Ca^{2+} oscillations and egg activation in mammals is a novel phospholipase C: PLCζ. Reproduction 127, 431–439.

Tasken, K., Aandahl, E.M., 2004. Localized effects of cAMP mediated by distinct routes of protein kinase A. Physiol. Rev. 84, 137–167.

Taylor, S.J., Exton, J.H., 1987. Guanine-nucleotide and hormone regulation of polyphosphoinositide phospholipase C activity of rat liver plasma membranes. Bivalent-cation and phospholipid requirements. Biochem. J. 248, 791–799.

Taylor, C.W., Rahman, T., Tovey, S.C., Dedos, S.G., Taylor, E.J., Velamakanni, S., 2009. IP_3 receptors: some lessons from DT40 cells. Immunol. Rev. 231(1), 23–44.

Visconti, P.E., 2009. Understanding the molecular basis of sperm capacitation through kinase design. Proc. Natl. Acad. Sci. USA 106, 667–668.

Wagner, J., Keizer, J., 1994. Effects of rapid buffers on Ca^{2+} on diffusion and Ca^{2+} oscillations. Biophys. J. 67, 447–456.

Walensky, L.D., Snyder, S.H., 1995. Inositol 1,4,5-trisphosphate receptors selectively localized to the acrosomes of mammalian sperm. J. Cell Biol. 130, 857–869.

Washington, T.M., Blum, J.J., Reed, M.C., Conn, M.P., 2004. A mathematical model for LH release in response to continuous and pulsatile exposure of gonadotrophs to GnRH. Theor. Biol. Med. Model 1, 1–17.

Watras, J., Bezprozvanny, I., Ehrlich, B.E., 1991. Inositol 1,4,5-trisphosphate-gated channels in cerebellum, presence of multiple conductance states. Eur. J. Neurosci. 11, 3239–3245.

Wennemuth, G., Westenbroek, R.E., Xu, T., Hille, B., Babcock, D.F., 2000. $Ca_V 2.2$ and $Ca_V 2.3$(N- and R-type) Ca^{2+} channels in depolarization-evoked entry of Ca^{2+} into mouse sperm. Int. J. Biol. Chem. 275, 21210–21217.

Wennemuth, G., Babcock, D.F., Hille, B., 2003. Calcium clearance mechanisms of mouse sperm. J. Gen. Physiol. 122, 115–128.

Wuytack, F., Raeymaekers, L., Missiaen, L., 2002. Molecular physiology of the SERCA and SPCA pumps. Cell Calcium 32, 279–305.

Xia, J., Ren, D., 2009. Egg coat proteins activated calcium entry into mouse sperm via CATSPER channels. Biol. Reprod. 80, 1092–1098.

Xia, J., Reigada, D., Mitchell, C.H., Ren, D., 2007. CatSper channel-mediated Ca^{2+} entry into mouse sperm triggers a tail-to-head propagation. Biol. Reprod. 77, 551–559.